Applied Surface Science 362 (2016) 517–524

Contents lists available at ScienceDirect

Applied Surface Science

journal homepage: www.elsevier.com/locate/apsusc

Selective adsorption of cationic dyes from aqueous solution by polyoxometalate-based metal–organic framework composite

Xiaoxia Liu, Wenpeng Gong, Jing Luo, Chentao Zou, Yun Yang, Shuijin Yang*

Hubei Collaborative Innovation Center for Rare Metal Chemistry, Hubei Key Laboratory of Pollutant Analysis & Reuse Technology, College of Chemistry and Chemical Engineering, Hubei Normal University, Cihu Road No. 11, Huangshi 435002, China

ARTICLE INFO

Article history:
Received 18 August 2015
Received in revised form 24 October 2015
Accepted 15 November 2015
Available online 17 November 2015

Keywords:
Selectivity adsorption
Cationic dye
$H_6P_2W_{18}O_{62}$
Metal organic frameworks

ABSTRACT

A novel environmental friendly adsorbent $H_6P_2W_{18}O_{62}$/MOF-5 was synthesized by a simple one-step reaction under solvothermal conditions and characterized by XRD, FTIR, thermogravimetric analyses (TGA) and N_2 adsorption–desorption isotherms. The removal rate of $H_6P_2W_{18}O_{62}$/MOF-5 was quite greater (85%) than that of MOF-5 (almost zero), showing that the adsorption performance of porous MOF-5 can be improved through the modification of $H_6P_2W_{18}O_{62}$. Further study revealed that $H_6P_2W_{18}O_{62}$/MOF-5 exhibited a fast adsorption rate and selective adsorption ability towards the cationic dyes in aqueous solution. The removal rate was up to 97% for cationic dyes methylene blue (MB) and 68% for rhodamine B(Rhb) within 10 min. However, anionicdye methyl orange(MO) can only reach to 10%. The influences including initial concentration, contact time, initial solution pH and temperature of MB adsorption onto $H_6P_2W_{18}O_{62}$/MOF-5 were investigated in detail. The kinetic study indicated that the adsorption of MB onto $H_6P_2W_{18}O_{62}$/MOF-5 followed the pseudo second-order model well. The isotherm obtained from experimental data fitted the Langmuir model, yielding maximum adsorption capacity of 51.81 mg/g. The thermodynamic parameters analysis illustrated that the MB adsorption onto $H_6P_2W_{18}O_{62}$ immobilized MOF-5 was spontaneous and endothermic process. Besides, these results implied that designing a novel material polyoxometalate-based metal–organic frameworks is great potential for removing cationic organic pollutants and even extended to improve other specific application.

1. Introduction

With the rapid industrial development, the pollution of water is becoming more and more serious resulting in the shortage in water supply [1]. Dyes are color organic compounds and widely used in the synthesis, textile, cosmetic, leather, printing, paper, food and other industries [2–4]. So far, more than 7×10^5 t year^{-1} and 10,000 different types of dyes are produced all over the world. To be sure, 10% to 15% of the dye is discharged due to washing operations and incomplete exhaustion of coloring materials during the dyeing process [5], which poses a significant threat to environment and human health because of their toxicity, potential mutagenicity, and even carcinogenicity without reasonably processing [6–8]. Moreover, the discharge of the dyes without treatment into the rivers is easily noticed since dyes are highly visible, which is commonly harmful to aquatic life [9,10]. Therefore, it is necessary to find appropriate treatment strategies for efficient removal of dyes from waste-water system before their discharge.

So far, there are many techniques which have been reported on the effective elimination of hazardous substances from aqueous solutions such as biological methods, physical, chemical, electrocoagulation, photocatalytic degradation, oxidation and so on [11–15]. Among the proposed techniques, adsorption is the procedure of choice and can reach good results as it is highly efficient, inexpensive and simple in operation [16–18]. This has encouraged the exploration of adsorbents with abundant availability and good economy. Nowadays a huge amount of low cost adsorbents are investigated including the common adsorbents, products of industrial or agricultural origin such as activated carbon [19], carbon nanotubes [20], activated slag, sugarcane, wood dust, fruit peel [21], tea waste ash, rice husk [22], metal–organic frameworks(MOFs) [23,24] and so on. However, there is still a great need to explore some kinds of new and low cost adsorbents with high adsorption capacity, even high selectivity and short contact time towards specific dyes [25].

Recently, the adsorbents with a high selectivity towards targeted dyes have attracted more and more researchers' interests due

* Corresponding author. Tel.: +86 0714 6515602.
E-mail address: yangshuijin@163.com (S. Yang).

http://dx.doi.org/10.1016/j.apsusc.2015.11.151
0169-4332/

to their huge potentiality in the controlled separation of dye mixtures and chemicals during treating industrial wastewater, as well as making sensors for the detection and identification of certain types of dyes [26]. MOFs fabricated by metal ions or metallic clusters connected through organic ligands by strong bonds are a new class of porous crystalline organic-inorganic hybrid materials [27]. Compared with conventional inorganic porous materials, MOFs have some unique features such as ultrahigh porosity, incredibly large BET surface area, multiple coordination sites, big pore volume and structural adaptivity, which brings many various potential applications such as gas separation and storage, sensors, energy storage, pollutant removal, catalysis, drug delivery and so on [28,29]. So many researches have been aimed at designing new MOFs structures and studying their various applications during the past two decades [30]. However, MOFs also exhibit several weak points such as the relative low stability in solution and brittleness or lack of flexibility hampering their realistic applications. It is necessary to introduce a new functionality for enhancing their realistic properties.

Wells–Dawson acids $H_6P_2W_{18}O_{62}$, one of the polyoxometalate (POM), possesses controllable shape and size, remarkable stability both in the solid state and in solution [31], oxo-enriched and highly negatively charged surfaces. These properties make them suitable to be used in selective adsorption and separation towards cationic dyes due to exerting a stronger electrostatic attraction to cationic dyes than anionic dyes [32]. However, $H_6P_2W_{18}O_{62}$ with feasible dissolution in water or polar organic liquids and relatively low surface area (<10 $m^2\,g^{-1}$) also limits its applications by preventing the accessibility to the active sites. In recent years, POM-based MOFs composite has been explored and used in the fields of various catalytic reactions such as the hydrolysis of esters [33], Knoevenagel condensation of benzaldehyde with ethyl cyanoacetate [34], and so on. Nevertheless, POM-based inorganic-organic hybrid material may also be a reasonable choice as a new type of adsorbent for removing cationic dyes. Recently, there have been two reports involved in the use of POM@MOFs composite as adsorbent in Wang's group and Sun's group [35,36]. Besides, POM-based materials in the adsorption application have not been still investigated up to now.

Here a new selective adsorbent $H_6P_2W_{18}O_{62}$/MOF-5 was prepared by a simple one-step solvothermal method. The adsorption of MB onto $H_6P_2W_{18}O_{62}$/MOF-5 about the effects of initial concentration, contact time, initial solution pH and temperature in the system was systematically explored. The composite exhibited a high adsorption rate and selective adsorption ability for the cationic dyes like MB compared to that of the isolated MOF-5 framework. Moreover, the adsorption isotherm, kinetic, adsorption mechanism and thermodynamic parameters of MB on the composite were thoroughly analyzed.

2. Experimental

2.1. Preparation of $H_6P_2W_{18}O_{62}$/MOF-5 adsorbents

Wells–Dawson acids $H_6P_2W_{18}O_{62}$ was prepared based on the method as in ref. [37] with some modifications. 50 g of $Na_2WO_4{\cdot}2H_2O$ (AR, Sinopharm Chemical Reagent Co., Ltd, Shanghai, China) was dissolved into 60 mL deionized water and 35 mL of phosphoric acid (H_3PO_4, 85%) was slowly added dropwise into the solution under vigorous stirring. Then the mixture was refluxed at 120 °C for 8 h. After cooling, HCl (22.5 mL, 36%) was added and the acidified aqueous solution was extracted by the same volume of ether as the solution. The heavy oily layer was collected and the ether was removed by heating gently. Finally, after drying under room temperature, heteropolyacid was obtained.

MOF-5 was prepared by a solvothermal method as in ref. [38]. $H_6P_2W_{18}O_{62}$/MOF-5 adsorbent was synthesized by the same method just like the above mention. 0.0166 g 1,4-dicarboxybenzene (H_2BDC, Tianjin Kwangfu Fine Chemical Industry Research Institute, Tianjin, China) was dissolved into 15 mL *N*,*N*-dimethylformamide (DMF) and stirred for 10 min till a homogeneous solution was formed. Then 0.149 g $Zn(NO_3)_2{\cdot}6H_2O$ and 0.05 g $H_6P_2W_{18}O_{62}$ were added into the solution with stirring continuously to form a clear mixed solution. Subsequently, the reactant mixture was loaded into a Teflon-lined stainless steel autoclave with 25 mL capacity and heated at 393 K for 21 h. The resulting white microcrystals were washed with a DMF/H_2O mixture at least five times and then dried under vacuum at 353 K overnight. Thus, $H_6P_2W_{18}O_{62}$/MOF-5 was obtained for further experiments.

2.2. Characterization

The $H_6P_2W_{18}O_{62}$, MOF-5 and $H_6P_2W_{18}O_{62}$/MOF-5 were characterized by XRD, TGA and FT-IR. X-ray powder diffraction patterns of the samples were collected on a diffractometer (Bruker Corporation) with the Cu $K\alpha$ radiation (40 kV, 40 mA) at a scanning rate of 0.02° s^{-1} and 2θ ranging from 5 to 40°. Thermogravimetric analyses (TGA) of $H_6P_2W_{18}O_{62}$/MOF-5 were performed using a thermogravimetric analyzer PERKIN ELMER at a heating rate of 5 K min^{-1} and temperature ranging from 25 °C to 800 °C in a flowing atmosphere of N_2. Functional groups of the samples were analyzed by a NICOLET 5700 FT-IR spectrometer within the wave range 4,000–500 cm^{-1}. The surface area (BET) and pore diameter of MOF-5 and $H_6P_2W_{18}O_{62}$/MOF-5 were determined from the N_2 adsorption at 77 K using a Micrometric ASAP 2020 system.

2.3. Dye adsorption experiments

In order to explore the adsorption properties and the factors influencing adsorption, batch adsorption experiments of MB (Beijing Chemical Reagent Co., Ltd, China) were conducted by using 50 mL reagent bottles with definite volume at different initial concentration under strong agitation. The solution pH was adjusted by using a certain amount of NaOH and HNO_3 solution. After adsorption, the mixture solution was centrifuged at 10000 rpm for 2 min and the concentration of residual MB was determined by using a UV–vis spectrophotometer (U-3010) at the maximum wavelength of 664 nm. The adsorption capacity q_t (mg g^{-1}) and removal rate (Removal%) were calculated according to the following equations:

$$q_t = \frac{(C_o - C_t)V}{m} \quad (1)$$

$$\text{Removal\%} = \frac{(C_o - C_t)100}{C_o} = \frac{(A_o - A_t)100}{A_o} \quad (2)$$

where C_o and C_t (mg L^{-1}) were the MB initial concentration and at time t. A_o and A_t represented the absorbance of MB before and after the adsorption. V (mL) was the volume of the MB solution and m (mg) was the mass of adsorbents.

3. Results and discussion

3.1. Characterization of the $H_6P_2W_{18}O_{62}$/MOF-5

The powder XRD patterns of MOF-5, $H_6P_2W_{18}O_{62}$ and $H_6P_2W_{18}O_{62}$/MOF-5 were shown in Fig. 1a. The characteristic diffraction peaks of MOF-5 implying the high crystallinity were consistent with the earlier reported literature well [39]. For $H_6P_2W_{18}O_{62}$, the peaks at 2θ = 7–10°, 14–19°, 24–30° matched well with Dawson structure as reported in the literature [40]. The diffraction patterns of the $H_6P_2W_{18}O_{62}$/MOF-5 composite were

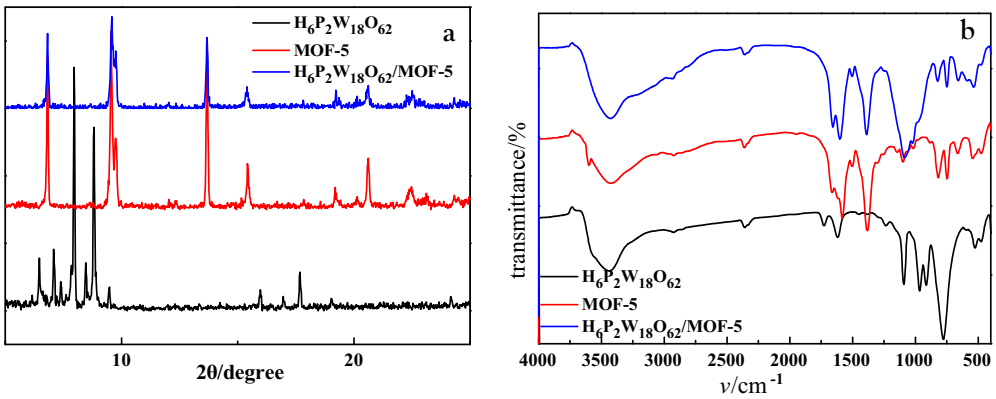

Fig. 1. XRD patterns (a) and FT-IR spectra (b) of $H_6P_2W_{18}O_{62}$, MOF-5 and $H_6P_2W_{18}O_{62}$/MOF-5.

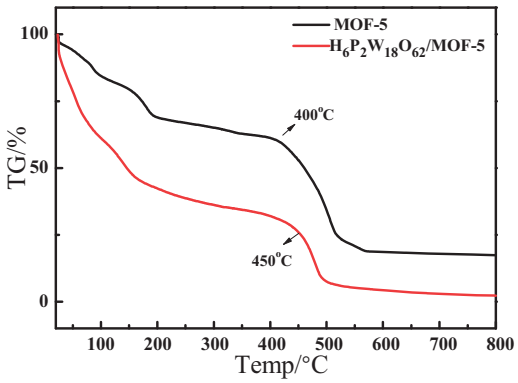

Fig. 2. TG-DTG-DTA profile of MOF-5 and $H_6P_2W_{18}O_{62}$/MOF-5.

almost the same as that observed for MOF-5 and no peaks of $H_6P_2W_{18}O_{62}$ were detected just like the literature [41]. However, the intensity of the peaks of the composite decreased apparently, indicating that the crystal structure remained unchanged even after forming the composite, in clear similar to the results reported by Gascon et al. [34]. Combined with the FT-IR results in Fig. 1b, the characteristic absorption peaks of $H_6P_2W_{18}O_{62}$ and MOF-5 agreed with the peaks reported in the literatures [23,42]. The characteristics peaks of MOF-5 were also observed in $H_6P_2W_{18}O_{62}$/MOF-5, further confirming the structure of MOF-5 was preserved. The characteristic peak at 962 cm^{-1} corresponded to υ_{as}(W=O$_d$) of $H_6P_2W_{18}O_{62}$ was observed in the composite and a wide peak at 1012 cm^{-1} appeared to be attributing to an effect of chemical interaction between $H_6P_2W_{18}O_{62}$ and MOF-5, indicating that the structure of $H_6P_2W_{18}O_{62}$ was also preserved in the composite $H_6P_2W_{18}O_{62}$/MOF-5.

Fig. 2 showed the two main steps of the weight loss for both MOF-5 and $H_6P_2W_{18}O_{62}$/MOF-5 with the increase of the temperature. The first weight loss steps between room temperature to 160 °C can be attributed to the removal of guest molecules, physically adsorbed water and crystal water. The second step was related to the collapse of the structures for both samples. Compared to the pure MOF-5, the second stage of $H_6P_2W_{18}O_{62}$/MOF-5 occurred at higher temperature. This may be explained that $H_6P_2W_{18}O_{62}$ should locate in the pure MOF-5 framework [38].

Nitrogen adsorption experiments were used to evaluate the pore size and structure of MOF-5 and $H_6P_2W_{18}O_{62}$/MOF-5. As seen in Fig. 3a, the samples both showed typical mesoporous character with adsorption curve of type IV. H4 type hysteresis loops at high relative pressure (P/Po range 0.80–1.00) can be ascribed to the presence of mesopores corresponding to the pore size distribution of both materials in Fig. 3b [43]. It can be found that the main

Table 1
Textural properties of MOF-5 and $H_6P_2W_{18}O_{62}$/MOF-5.

Sample	S_{BET} (m^2 g^{-1})	V_{total} (cm^3 g^{-1})	D (nm)
MOF-5	92	0.0729	3.19
$H_6P_2W_{18}O_{62}$/MOF-5	395	0.2986	3.03

S_{BET}: BET surface area. V_{total}: Total pore volume. D: Average pore diameter calculated using BJH method.

pore distributions were both in a wide pore size of 10–30 nm range, conformed with the value of 16 nm calculated by BJH model from N_2 adsorption isotherms. Some textural properties of the samples were listed in Table 1. As shown in Table 1, the materials were mesoporous (average pore diameter is approximately 3 nm). The BET surface area and pore volume of $H_6P_2W_{18}O_{62}$/MOF-5 were higher than the values of MOF-5. It can be concluded that the addition of $H_6P_2W_{18}O_{62}$ had a great effect on the structure of MOF-5, greatly increasing the surface area and pore volume, which were all favorable factors for improving the adsorption performance.

3.2. MB adsorption

3.2.1. Effects of initial pH

The solution pH has been identified as a rather significant variable enhancing or depressing the adsorption uptake of adsorbate molecules, which is attributed to influencing surface binding-sites or charges of the adsorbent and the degree of ionization/dissociation of dye molecules [44]. The effect of initial solution pH on MB adsorption onto $H_6P_2W_{18}O_{62}$/MOF-5 was investigated in the pH range from 2 to 10 (Fig. 4). Fig. 4a showed that the absorbances recorded by the UV/Vis adsorption spectrum increased with the increase of pH, indicating that the residual concentrations of MB in the solution were larger at high pH. Moreover, it is obvious that the adsorption capacity and removal rate can reach 26.92 mg g^{-1} and 100% at low pH in Fig. 4b, respectively, further suggesting that acidic solutions benefited MB adsorption. This phenomenon can be explained that POM with highly electronegative possessed a good adsorption and selective separation ability towards the cationic dyes [36]. According to the point-of-zero charge (pH$_{PZC}$) of the composite, the surface charge was all negative at the pH range from 2 to 10, which conforms to the above explanation. With increasing the initial pH, the adsorption capacity and removal rate were both becoming small. One explanation for this observation is that chloride anion in MB was exchanged with NaOH to have a displacement reaction, forming NaCl (aq) and MBS + OH (aq). However, the salt of NaCl might result in the deactivation of $H_6P_2W_{18}O_{62}$/MOF-5 and decrease the adsorption of MBS + OH (aq) on the $H_6P_2W_{18}O_{62}$/MOF-5 at last [24].

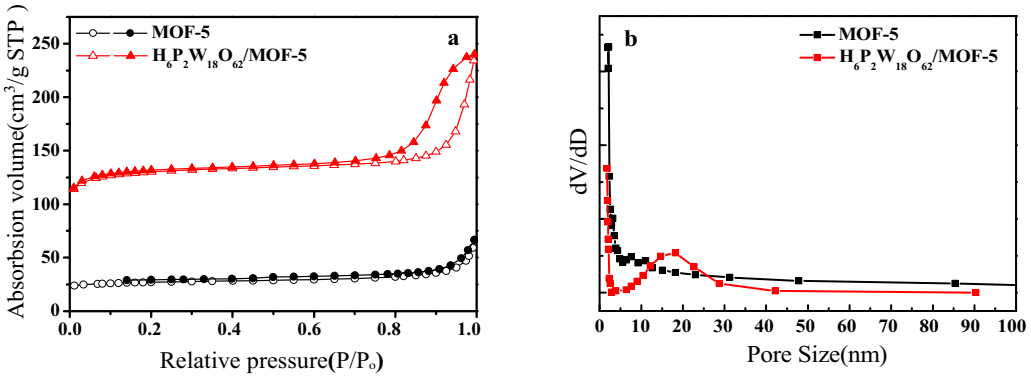

Fig. 3. N_2 adsorption–desorption isotherms (a) and pore size distribution curve (b) of MOF-5 and $H_6P_2W_{18}O_{62}$/MOF-5.

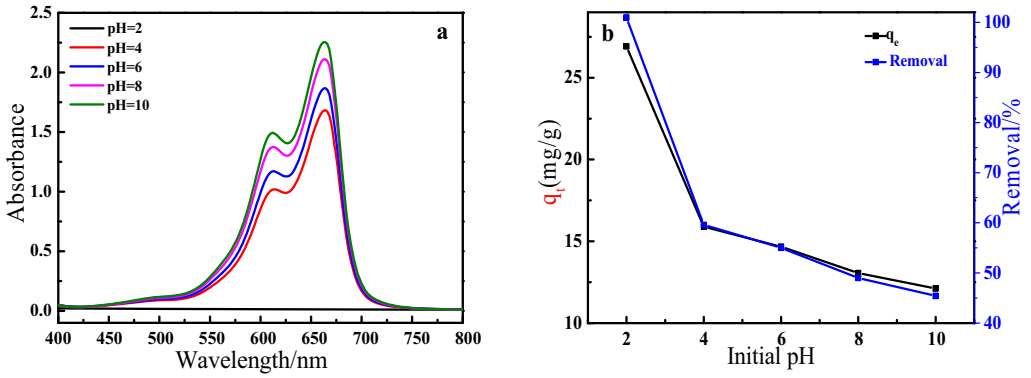

Fig. 4. Effect of pH on adsorption capability and removal rate of MB. (T = 293 K; m = 15 mg; V = 20 mL, Co = 20 mg L^{-1}, t = 10 min).

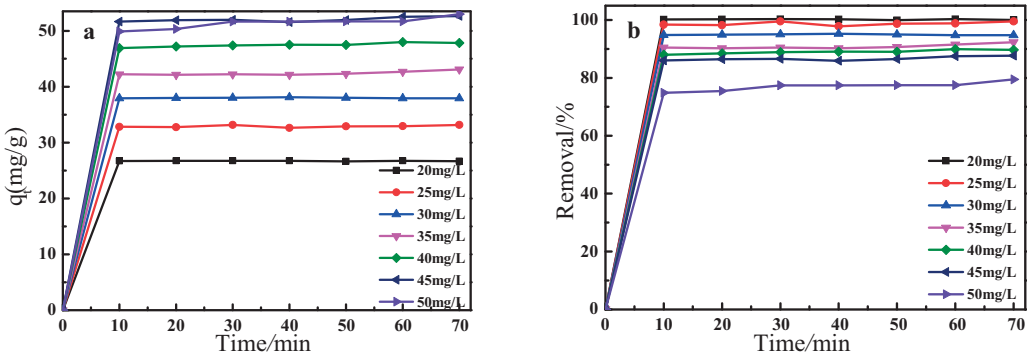

Fig. 5. (a,b) Effects of initial concentration and contact time on the adsorption of MB (experimental conditions: initial dye concentration: 20–45 (20, 25, 30, 35, 40, 45, 50) mg L^{-1}, contact time: 10–70 (10, 20, 30, 40, 50, 60, 70) min, temperature: 293 K, adsorbent dose: 15 mg/20 mL).

3.2.2. *Effect of initial concentration and contact time*

The effects of the different initial concentration and contact time on the adsorption of MB onto the complexes were shown in Fig. 5a and b. It is obvious that the adsorption capacity increased gradually from 26.75 to 52.65 mg g^{-1} with the increase of the initial concentration of MB. However, the removal rate of the composite towards MB can reach up to 90% at the lower initial concentration (20, 25 and 30 mg L^{-1}). Besides, the adsorption process could reach an equilibrium state in the first 10 min and then be constant for all the samples due to most available vacant surface sites in the $H_6P_2W_{18}O_{62}$/MOF-5 during the initial stage, indicating the complexes especially suitable for rapid removing MB from aqueous solutions. Moreover, there was little increase for the adsorption capacity corresponding initial concentration of MB from 45 to 50 mg L^{-1}, which indicated that a saturable adsorption capacity has been attained and the initial concentration was one of the critical parameters affecting the adsorption property of an adsorbent in waste water treatment systems.

3.2.3. *Effect of temperature*

The temperature played an important role on the process of MB adsorption onto $H_6P_2W_{18}O_{62}$/MOF-5 and the results of the effect were shown in Fig. 6. The saturated adsorption capacity of MB was found to increase with increasing temperature, indicating that the dye adsorption onto $H_6P_2W_{18}O_{62}$/MOF-5 was favored at high temperature and further revealing that the adsorption process was endothermic. One explanation for the phenomenon is that the viscosity of the solution decreased at high temperature, resulting in an increasing rate of the adsorbate molecule diffusion between the external boundary layer and internal pores in the adsorbent [45]. On the other hand, the increasing temperature may prohibit the

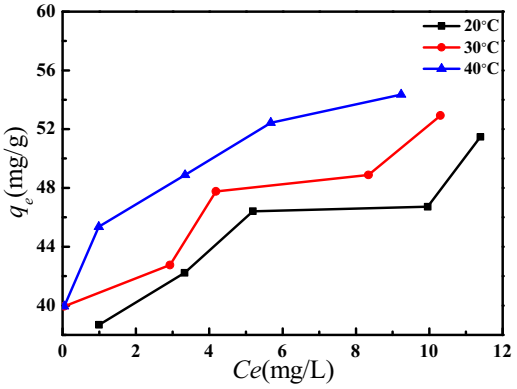

Fig. 6. Effect of temperature on the adsorption of MB (*Co*: 30–50 mg L^{-1}, adsorbent dose: 15 mg/20 mL, pH = 2, *t* = 3 h).

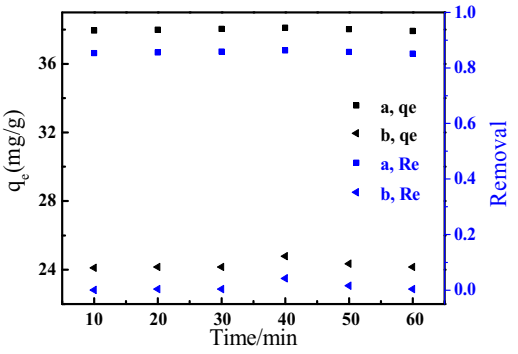

Fig. 7. Comparison of adsorption capacity and removal rate for MB in pure $H_6P_2W_{18}O_{62}$/MOF-5 (a) and MOF-5 (b) (*Co*: 30 mg L^{-1}, adsorbent dose: 15 mg/20 mL, pH = 2, *t* = 60 min).

conglomeration of adsorbent or adsorbate and be the benefit of the uptake of MB.

3.2.4. Comparison of adsorption ability for MB in pure MOF-5 and $H_6P_2W_{18}O_{62}$/MOF-5

The adsorption capacity and removal rate of pure MOF-5 and $H_6P_2W_{18}O_{62}$/MOF-5 for MB were compared as shown in Fig. 7. Obviously, the adsorption capacity of two materials both quickly reached equilibrium state within 10 min. Compared with $H_6P_2W_{18}O_{62}$/MOF-5, the adsorption capacity of pure MOF-5 was much smaller than that of the composite and the removal rate was nearly zero. The removal rate of the composite was up to 85% within 10 min. So there is still significant value in exploring the composite $H_6P_2W_{18}O_{62}$/MOF-5 as a kind of new adsorbent.

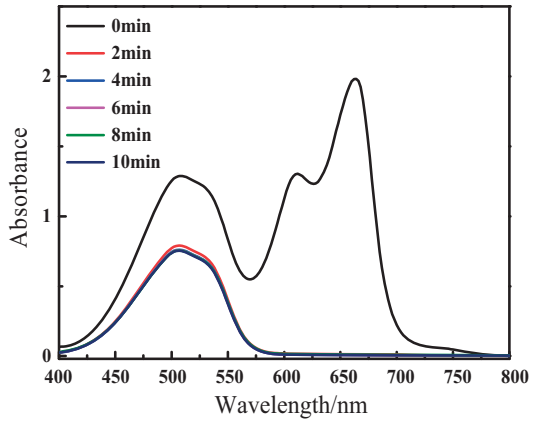

Fig. 9. The selective adsorption capability of $H_6P_2W_{18}O_{62}$/MOF-5 toward the mixed dyes solution with MB and MO (experiment conditions: C_0(MB): 10 mg L^{-1}, C_0(MO): 10 mg L^{-1}, adsorbent dose: 15 mg/20 mL, pH = 2).

3.2.5. Selective adsorption ability

With developing of industry, a high selectivity towards different kinds of dyes has drawn great attention during the process of treating industrial waste water. So it is necessary to explore the selective adsorption ability for some materials as the adsorbents. As shown in Fig. 8a and b, the composite exhibited better adsorption ability towards MB and Rhb instead of MO combined with Fig. 4a. Fig. 8c revealed that the removal rate was up to 97 and 68% within 10 min for cationic dyes MB and Rhb. However, anionicdye MO can only reach to 10%. It could be further deduced that POM with much negative charges played a major role in the adsorption process due to its stronger force with electropositive dyes.

Considering that the real wastewater can not only contain a single component. So the mixed dye solution with MB and MO was selected as the simulated real wastewater systems to explore the industrial application of the composite and its separation ability in the mixed dye molecules. As shown in Fig. 9, the absorption peaks of MB almost disappeared within 2 min in the UV/vis absorption spectra, but the characteristic absorption peaks of MO slowed down small, indicating that the composite could selectively and quickly separate MB in the multi-component wastewater systems.

3.3. Adsorption kinetics

In order to understand the adsorption behaviors including adsorption mechanism and rate, the kinetic models including pseudo-first-order and pseudo-second-order rate equations were used to analyze the data obtained at different initial concentrations

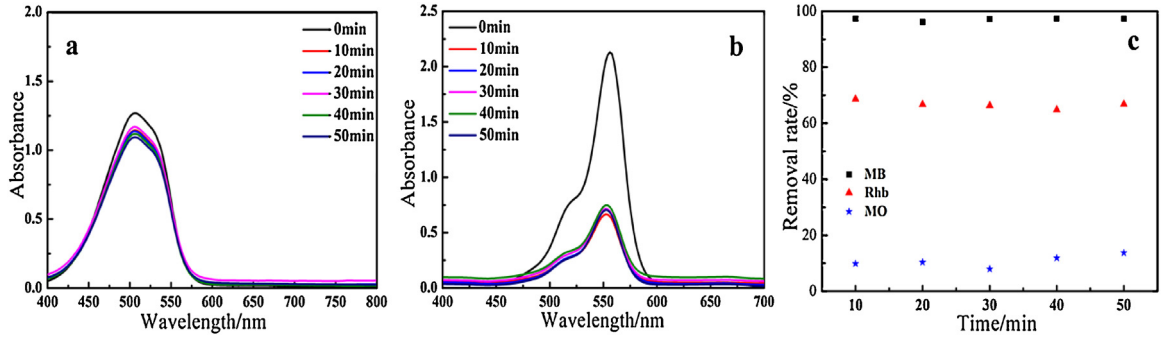

Fig. 8. The adsorption capability of $H_6P_2W_{18}O_{62}$/MOF-5 toward MO (a), Rhb (b) and the removal rate of Rhb, MO and MB (c) (experiment conditions: C_0: 10 mg L^{-1}, adsorbent dose: 15 mg/20 mL, pH = 2, *t* = 50 min).

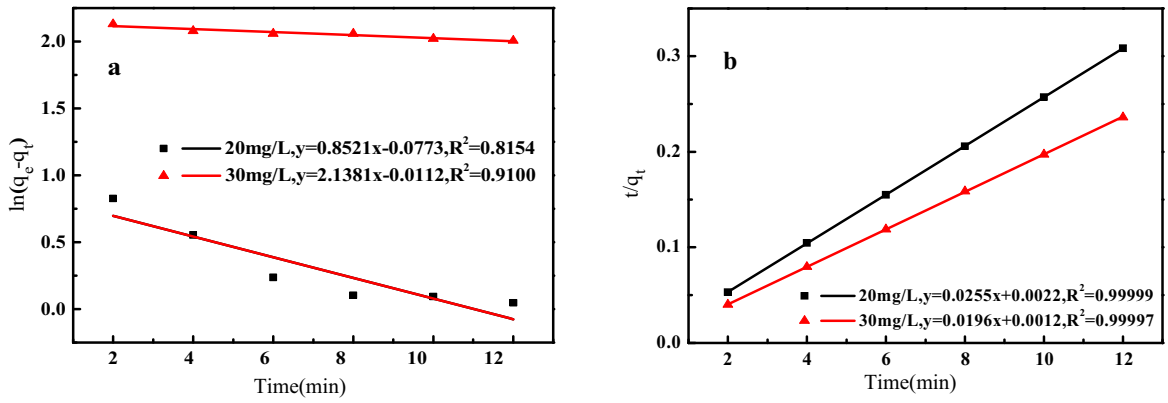

Fig. 10. Plots of pseudo-first-order (a) and pseudo-second-order (b) kinetics for the adsorption of MB on $H_6P_2W_{18}O_{62}$/MOF-5 (Co = 20, 30 mg L^{-1}, adsorbent dose: 5 mg/10 mL, pH = 2).

Table 2
Kinetic parameters and correlation coefficients for the pseudo first-order equation and pseudo second-order equation.

Kinetics model	Initial concentration (mg L^{-1})	$q_{e,exp}$ (mg g^{-1})	$q_{e,cal}$ (mg g^{-1})	k_1 (min^{-1}) k_2 (mg g^{-1} min^{-1})	R^2
Pseudo-first-order model	20	39.98	2.3446	0.0773	0.8154
	30	58.26	8.4833	0.0112	0.9100
Pseudo-second-order model	20	39.98	39.22	0.2953	0.99999
	30	58.26	51.02	0.3232	0.99997

of MB (20 and 30 mg L^{-1}). The two linear equations are commonly expressed as follows [46]:

$$\ln(q_e - q_t) = \ln q_e - k_1 t \quad (3)$$

$$\frac{t}{q_t} = \frac{1}{k_2 q_e^2} + \frac{1}{q_e} t \quad (4)$$

where q_e (mg g^{-1}) is the amount of adsorption at equilibrium state and q_t (mg g^{-1}) is at adsorption time t (min). k_1 (min^{-1}) named the Lagergren rate constant of adsorption can be calculated from the slope of the plot in Fig. 10a and was listed in Table 2. k_2 can be calculated according to k_2 = slope^2/intercept in the plot of Fig. 10b. The correlation coefficient R^2 values (0.99999 and 0.99997) determined by pseudo-second-order model were higher than that of pseudo-first-order model for both different initial concentrations of MB, indicating that the adsorption of MB onto $H_6P_2W_{18}O_{62}$/MOF-5 fitted the pseudo-second-order model well. Besides, the experimental q_e was much closer to the calculated q_e when analyzed by pseudo-second-order model, also illustrating this point.

3.4. Adsorption isotherms

Just to further describe the adsorption progress and investigate adsorption mechanisms, two isotherm models containing the Langmuir isotherm and the Freundlich isotherm to the adsorption behavior were used for this study, in which the experiments were conducted at three temperatures (293, 303 and 313 K). The Langmuir model supposes that the adsorption process occurs at homogeneous sites in the adsorbent surface and is monolayer in nature. As shown in Fig. 11a, the isotherms with the linear form have been plotted to fit the Langmuir equation [47]:

$$\frac{C_e}{q_e} = \frac{1}{q_m} C_e + \frac{1}{q_m K_L} \quad (5)$$

where C_e (mg L^{-1}) is the equilibrium concentration of adsorbate (mg L^{-1}). q_m (mg g^{-1}) named the maximum adsorption capacity and K_L (L g^{-1}) named Langmuir constant can be determined from the slope and intercept (Table 3). K_L is related to the energy of adsorption and affinity of the binding sites. The coefficients

Table 3
Langmuir and Freundlich isotherm parameters for the adsorption of MB onto $H_6P_2W_{18}O_{62}$/MOF-5.

Adsorption	Constant	293 K	303 K	313 K
Langmuir	$q_{m.c}$ (mg g^{-1})	51.81	52.83	54.79
	K_L (L g^{-1})	1.75	2.78	5.27
	R_L	0.0145	0.0092	0.0049
	R^2	0.9898	0.9908	0.9977
Freundlich	K_F (mg$^{1-1/n}$ g^{-1} $L^{1/n}$)	38.32	44.81	46.91
	n	9.56	23.93	18.20
	R^2	0.8670	0.6362	0.9366

Table 4
Comparison of adsorption capacity of various adsorbents for MB.

Materials	Adsorption capacity (q_e, mg g^{-1})	Ref.
Zn-MOF	0.75	[53]
MWCNTs/Fe_2O_3	42.3	[54]
Magnetic MWCNTs	48.1	[55]
Exfoliated graphene oxide	17.3	[56]
Carbon nanotubes	35.4	[57]
Zeolite	10.86	[58]
Polyaniline nanotubes	4.8	[59]
$H_6P_2W_{18}O_{62}$/MOF-5	51.81	This work

R^2 of the Langmuir equation showed that the adsorption of MB onto $H_6P_2W_{18}O_{62}$/MOF-5 fitted the Langmuir's model. The maximum uptake capacity of the composite at room temperature was 51.81 mg g^{-1} and considerably high compared to that of other materials towards MB reported in Table 4. The value of $q_{m.c}$ increased with the increasing temperature, indicating that the adsorption was favorable at high temperature and was an endothermic process. In order to further predict the favorability of the adsorption system, a dimensionless separation factor R_L has been introduced as follows [48]:

$$R_L = \frac{1}{1 + K_L C_o} \quad (6)$$

The parameter can indicate that the isotherm is irreversible (R_L = 0), favorable (0 < R_L < 1), linear (R_L = 1) or unfavorable (R_L > 1)

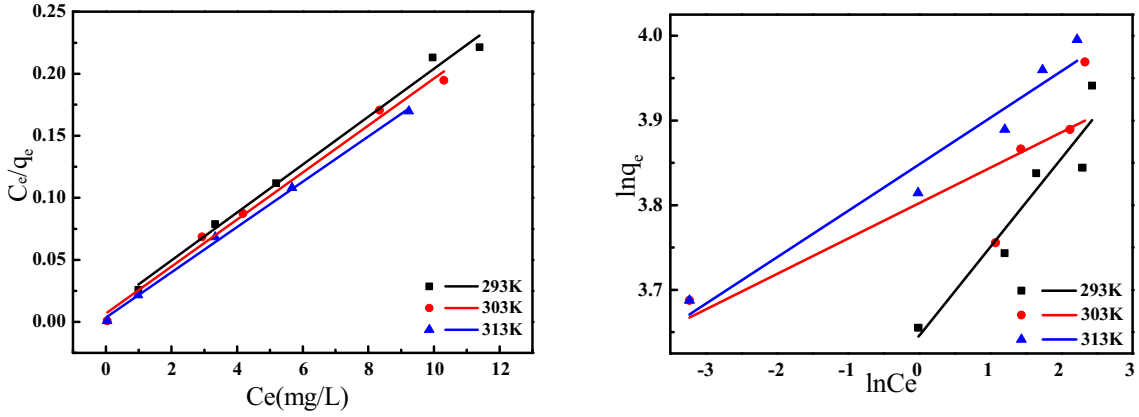

Fig. 11. Plots of the isotherms for MB adsorbed by $H_6P_2W_{18}O_{62}$/MOF-5: (a) the Langmuir isotherm, (b) the Freundlich isotherm.

Table 5
Thermodynamic parameters for the MB adsorption by $H_6P_2W_{18}O_{62}$/MOF-5.

T (K)	K_L	ΔG (kJ mol^{-1})	ΔH (kJ mol^{-1})	ΔS (J mol^{-1} K^{-1})
293	1.75	−1.3633	41.94	147.5
303	2.78	−2.5759		
313	5.27	−4.3253		

[49,50]. The R_L values in Table 3 were between 0 and 1, which illustrated that the adsorption of MB onto $H_6P_2W_{18}O_{62}$/MOF-5 was favorable.

The Freundlich isotherm is applicable to describe the adsorption capacity related to the dye concentration at equilibrium and the adsorption process taking place on a heterogeneous surface corresponding to a multilayer adsorption mechanism [51]. The isotherms (Fig. 11b) conforming to linear empirical Freundlich model have been plotted by equation as follows [52]:

$$\ln q_e = \frac{1}{n} \ln C_e + \ln K_F \tag{7}$$

where K_F is a Freundlich constant and n is the heterogeneity factor related to adsorption capacity and adsorption intensity. As shown in Table 3, they can be evaluated from the slope and intercept. It is quite clear that the adsorption fitted Langmuir model better than Freundlich model based on the R^2 values of the Freundlich equation.

3.5. Thermodynamic study

In order to further calculate the thermodynamic functions and the effect of temperature on the adsorption process of MB onto $H_6P_2W_{18}O_{62}$/MOF-5, Gibbs free energy ΔG°, enthalpy ΔH°, and entropy ΔS° about these thermodynamic parameters were calculated and listed in Table 5 by the following equations [60,61]

$$\Delta G^\circ = -RT \ln K_L \tag{8}$$

$$\ln K_L = \frac{\Delta S^\circ}{R} - \frac{\Delta H^\circ}{RT} \tag{9}$$

where K_L (L g^{-1}) is the Langmuir constant. R (8.314 J mol^{-1} K^{-1}) is gas constant and T (K) is the temperature. The negative values of ΔG° for different temperatures showed that the adsorption on the composites was a spontaneous process. Also, the parameter demonstrated that the adsorption process was physisorption ($-20\,\text{kJ mol}^{-1} < \Delta G^\circ < 0$) rather than chemisorption ($-80\,\text{kJ mol}^{-1} < \Delta G^\circ < -400\,\text{kJ mol}^{-1}$) [4,62]. The positive value of ΔH° indicated that the interaction of MB adsorbed by $H_6P_2W_{18}O_{62}$/MOF-5 was endothermic process in accord with the increasing adsorption capacity associated with the increase of temperature. The positive value of ΔS° increased the randomness at the solid-solute interface and the affinity of $H_6P_2W_{18}O_{62}$/MOF-5 for the MB [62].

4. Conclusions

In summary, a new adsorbent $H_6P_2W_{18}O_{62}$/MOF-5 was prepared by a simple one-pot solvothermal method and its adsorptive property of cationic dye MB has been investigated. The results showed that the adsorption efficiency of MOF-5 towards MB in aqueous solution was significantly improved by the modification of $H_6P_2W_{18}O_{62}$ and the composite $H_6P_2W_{18}O_{62}$/MOF-5 exhibited a rapid and selective adsorption ability towards the cationic dyes MB instead of anionic dye MO in aqueous solution. The experiment data could be well described by the Langmuir equations and pseudo-second-order kinetic model. Thermodynamic parameters $\Delta G^\circ < 0$ and $\Delta H^\circ > 0$ indicated that the MB adsorption onto $H_6P_2W_{18}O_{62}$/MOF-5 was spontaneous and endothermic. The results of removing dyes show that designing a novel material with specific application based on the POM and MOFs is a promising strategy.

Acknowledgments

This work was financially supported by the Natural Science Foundation of Hubei Province (No. 2014CFA131), National Undergraduate Training Programs for Innovation and Entrepreneurship (No. 201513256001) and Postgraduate Innovation Scientific Research Foundation of Hubei Normal University (No. 070301201302).

References

[1] T.A. Saleh, V.K. Gupta, Environ. Sci. Pollut. Rec. 19 (2012) 1224–1228.
[2] Y. Wang, M. Yao, Y. Chen, Y. Zuo, X. Zhang, L. Cui, J. Alloy. Compd. 627 (2015) 7–12.
[3] A.S. Özcan, B. Erdem, A. Özcan, J. Colloid Interface Sci. 280 (2004) 44–54.
[4] T.A. Khan, E.A. Khan, Shahjahan, Appl. Clay Sci. 107 (2015) 70–77.
[5] V.K. Gupta, R. Jain, A. Nayak, S. Agarwal, M. Shrivastava, Mater. Sci. Eng., C 31 (2011) 1062–1067.
[6] E.V. Datskevich, R.V. Prikhod'ko, I.V. Stolyarova, A.V. Lozovskii, V.V. Goncharuk, Russ. J. Appl. Chem. 83 (2010) 1785–1793.
[7] Z. Chen, J. Fu, M. Wang, X. Wang, J. Zhang, Q. Xu, Appl. Surf. Sci. 289 (2014) 495–501.
[8] Y. Li, Q. Du, T. Liu, J. Sun, Y. Wang, S. Wu, Z. Wang, Y. Xia, L. Xia, Carbohydr. Polym. 95 (2013) 501–507.
[9] C.A.P. Almeida, N.A. Debacher, A.J. Downs, L. Cottet, C.A.D. Mello, J. Colloid Interface Sci. 332 (2009) 46–53.
[10] A.T. Paulino, M.R. Guilherme, A.V. Reis, G.M. Campese, E.C. Muniz, J. Nozaki, J. Colloid Interface Sci. 301 (2006) 55–62.
[11] S. Karthikeyan, V.K. Gupta, R. Boopathy, A. Titus, G. Sekaran, J. Mol. Liq. 173 (2012) 153–163.
[12] Y. Liu, C. Luo, J. Sun, H. Li, Z. Sun, S. Yan, J. Mater. Chem., A 3 (2015) 5674–5682.

[13] T.A. Khan, M. Nazir, Environ. Prog. Sustain 34 (2015) 1444–1454.
[14] T.A. Saleh, V.K. Gupta, Adv. Colloid Interface Sci. 211 (2014) 93–101.
[15] T.A. Khan, M. Nazir, E.A. Khan, Toxicol. Environ. Chem. 95 (2013) 919–931.
[16] T.A. Khan, S.A. Chaudhry, I. Ali, J. Mol. Liq. 202 (2015) 165–175.
[17] Z. Chen, L. Zhou, F. Zhang, C. Yu, Z. Wei, Appl. Surf. Sci. 258 (2012) 5291–5298.
[18] T.A. Khan, V. Singh, I. Ali, J. Environ. Prot. Sci. 3 (2009) 124–132.
[19] B.H. Hameed, A.L. Ahmad, K.N.A. Latiff, Dyes Pigments 75 (2007) 143–149.
[20] V.K. Gupta, S. Agarwal, T.A. Saleh, J. Hazard. Mater. 185 (2011) 17–23.
[21] A. Mittal, D. Kaur, A. Malviya, J. Mittal, V.K. Gupta, J. Colloid Interface Sci. 337 (2009) 345–354.
[22] A. Mittal, J. Mittal, A. Malviya, D. Kaur, V.K. Gupta, J. Colloid Interface Sci. 342 (2010) 518–527.
[23] W. Dai, J. Hu, L. Zhou, S. Li, X. Hu, H. Huang, Energy Fuels 27 (2013) 816–821.
[24] S. Lin, Z. Song, G. Che, A. Ren, P. Li, C. Liu, J. Zhang, Microporous Mesoporous Mater. 193 (2014) 27–34.
[25] T.A. Khan, M. Nazir, I. Ali, A. Kumar, Arab. J. Chem. (2013), http://dx.doi.org/10.1016/j.arabjc.2013.08.019.
[26] W. Wei, R. Lu, H. Xie, Y. Zhang, X. Bai, L. Gu, R. Da, X. Liu, J. Mater. Chem., A 3 (2015) 4314–4322.
[27] T.R. Cook, Y.R. Zheng, P.J. Stang, Chem. Rev. 113 (2012) 734–777.
[28] F. Ke, L.G. Qiu, Y.P. Yuan, F. Peng, X. Jiang, A. Xie, Y. Shen, J. Zhu, J. Hazard. Mater. 196 (2011) 36–43.
[29] N. Stock, S. Biswas, Chem. Rev. 112 (2011) 933–969.
[30] Q.L. Zhu, Q. Xu, Chem. Soc. Rev. 43 (2014) 5468–5512.
[31] L.E. Briand, G.T. Baronetti, H.J. Thomas, Appl. Catal., A: Gen. 256 (2003) 37–50.
[32] A. Çelekli, H. Bozkurt, Environ. Sci. Pollut. Res. 20 (2013) 4647–4658.
[33] C. Sun, S. Liu, D. Liang, K. Shao, Y. Ren, Z. Su, J. Am. Chem. Soc. 131 (2009) 1883–1888.
[34] J. Juan-Alcañiz, E.V. Ramos-Fernandez, U. Lafont, J. Gascon, F. Kapteijn, J. Catal. 269 (2010) 229–241.
[35] A.X. Yan, S. Yao, Y.G. Li, Z. Zhang, Y. Lu, W. Chen, E. Wang, Chem. Eur. J. 20 (2014) 6927–6933.
[36] F. Yi, W. Zhu, S. Dang, J. Li, D. Wu, Y. Li, Z. Sun, Chem. Commun. 51 (2015) 3336–3339.
[37] D.K. Lyon, W.K. Miller, T. Novet, J. Am. Chem. Soc. 113 (1991) 7209–7221.
[38] H. Li, W. Shi, K. Zhao, H. Li, Y. Bing, P. Cheng, Inorg. Chem. 51 (2012) 9200–9207.
[39] C. Mckinstry, E.J. Cussen, A.J. Fletcher, S.V. Patwardhan, J. Sefcik, Cryst. Growth Des. 13 (2013) 5481–5486.
[40] Z.L. Fan, X.R. Wang, G.X. Li, Chin. J. Mol. Catal. 26 (2012) 32–38.
[41] L.H. Wee, S.R. Bajpe, N. Janssens, I. Hermans, K. Houthoofd, C.E.A. Kirschhock, J.A. Martens, Chem. Commun. 46 (2010) 8186–8188.
[42] A. Bielański, A. Lubańska, J. Mol. Catal., A: Chem. 224 (2004) 179–187.
[43] T. Chen, Y. Che, Y. Zhang, J. Zhang, F. Wang, Z. Wang, J. Porous Mater. 21 (2014) 495–502.
[44] Z. Chen, J. Zhang, J. Fu, M. Wang, X. Wang, R. Han, Q. Xu, J. Hazard. Mater. 273 (2014) 263–271.
[45] S. Karaca, A. Gürses, M. Açıkyıldız, M. Ejder (Korucu), Microporous Mesoporous Mater. 115 (2008) 376–382.
[46] P.M.K. Reddy, S.K. Mahammadunnisa, B. Ramaraju, B. Sreedhar, C. Subrahmanyam, Environ. Sci. Pollut. Res. 20 (2013) 4111–4124.
[47] Y. Ho, W. Chiu, C. Wang, Bioresour. Technol. 96 (2005) 1285–1291.
[48] F. Zhang, W. Song, J. Lan, Appl. Surf. Sci. 326 (2015) 195–203.
[49] M. Chen, Y. Chen, G. Diao, J. Chem. Eng. Data 55 (2010) 5109–5116.
[50] Z. Ding, W. Wang, Y. Zhang, F. Li, J. Liu, J. Alloy. Compd. 640 (2015) 362–370.
[51] G. Hao, W. Li, S. Wang, S. Zhang, A. Lu, Carbon 48 (2010) 3330–3339.
[52] T. Liu, Y. Li, Q. Du, J. Sun, Y. Jiao, G. Yang, Z. Wang, Y. Xia, W. Zhang, K. Wang, H. Zhu, D. Wu, Colloid Surf., B: Biointerfaces 90 (2012) 197–203.
[53] C. Sun, X. Wang, C. Qin, J. Jin, Z. Su, P. Huang, K. Shao, Chem. Eur. J. 19 (2013) 3639–3645.
[54] S. Qu, F. Huang, S. Yu, G. Chen, J. Kong, J. Hazard. Mater. 160 (2008) 643–647.
[55] L. Ai, C. Zhang, F. Liao, Y. Wang, M. Li, L. Meng, J. Jiang, J. Hazard. Mater. 198 (2011) 282–290.
[56] G.K. Ramesha, A.V. Kumara, H.B. Muralidhara, S. Sampath, J. Colloid Interface Sci. 361 (2011) 270–277.
[57] Y.J. Yao, F.F. Xu, M. Chen, Z.X. Xu, Z.W. Zhu, Bioresour. Technol. 101 (2010) 3040–3046.
[58] C. Woolard, J. Strong, C. Erasmus, Appl. Geochem. 17 (2002) 1159–1164.
[59] M.M. Ayad, A.A. El-Nasr, J. Phys. Chem., C 114 (2010) 14377–14383.
[60] A.A. Olajire, A.A. Giwa, I.A. Bello, Int. J. Environ. Sci. Technol. 12 (2015) 939–950.
[61] S. Song, Y. Ma, H. Shen, M. Zhang, Z. Zhang, RSC Adv. 5 (2015) 27922–27932.
[62] A.N. Fernandes, C.A.P. Almeida, N.A. Debacher, J. Mol. Struct. 982 (2010) 62–65.